Structural transformation and oxidation of $Sr_2MnO_{3.5+x}$ determined by *in-situ* neutron powder diffraction

C. N. Munnings, R. Sayers, P.A. Stuart and S.J. Skinner*

Department of Materials, Imperial College London, Prince Consort Road, London, SW7 2BP, UK

Abstract

The oxidation of the n=1 Ruddlesden-Popper phase, $Sr_2MnO_{3.5+x}$, where $0 \leq x \leq 0.5$ has been investigated using a combination of *in-situ* diffraction techniques. In agreement with previous reports the room temperature structure of $Sr_2MnO_{3.5+x}$ was determined to be monoclinic crystallising in space group $P2_1/c$. On heating in air the material undergoes rapid oxidation at a relatively modest temperature, ~275^{o}C. The oxidation process is coincident with a significant change in the structure, with the material now adopting a tetragonal *I4/mmm* structure. In the oxygen deficient phase where $x > 0$ the Mn coordination is square pyramidal, with a sixth partially occupied oxygen position giving rise to octahedral coordination. Oxidation of $Sr_2MnO_{3.5+x}$ results in the filling of the partially occupied O4 positions and a resulting increase in symmetry, with the Mn coordination now adopting solely a distorted octahedral environment.

Keywords: $Sr_2MnO_{3.5+x}$, neutron diffraction, in-situ, oxidation

* Corresponding Author
Tel: +44 (0)20 7594 6782
Fax: +44 (0)20 7594 6757
Email: s.skinner@imperial.ac.uk

1. Introduction

With increasing awareness of the demand to reduce gaseous emissions, such as CO_2, and to generate power with greater efficiency using non-fossil fuel resources, there has been increased interest in electrochemical technologies such as fuel cells, permeation membranes and electrolysers based on oxides with fast oxide ion conduction. Indeed the layered perovskites of the K_2NiF_4 type have proven to be among the most promising new materials developed. As well as their applicability for electrochemical cells there are a number of other technology areas to which the K_2NiF_4 type oxides are suited.

Oxides of the K_2NiF_4 structure type are of interest for a number of technological applications and as such many studies have investigated the magnetic, electronic and structural properties of a wide range of compositions over a large temperature range[1-10]. Much of the earlier work was concerned with the low temperature behaviour of the La_2CuO_4[11-13] and La_2NiO_4[14] materials and their potential use in superconducting applications. Further interest in this class of materials was generated by the discovery of colossal magnetoresistance in Mn based materials[15, 16], and significant efforts were directed towards the development of a wide range of Mn based perovskites[9, 15-17] including La-Sr-Mn-O, $SrMnO_3$ and Sr_2MnO_{4-d}. Much of this effort has concentrated on the determination of the structural chemistry of these and related phases.

Sr_2MnO_{4-d} has been determined by several authors to undergo phase transformations as the oxygen content varies, thus altering the Mn valence and hence the Mn-O bond lengths, as well as the electrical properties. It has been widely reported that $Sr_2MnO_{3.5}$ exists and will oxidise to a stoichiometry of Sr_2MnO_4, depending upon conditions[18-21]. Through substitution on the Sr site with La and careful control of the synthesis conditions an oxygen hyperstoichiometry of x = 0.27 can be achieved in the $La_{1.2}Sr_{0.8}MnO_{4+x}$ material[22]. Initially it was reported that the Sr_2MnO_{4-d} materials adopted the tetragonal I4/mmm space group with a long c-axis[23], but more recently Gillie et al[19] refined the oxygen deficient materials within the $P2_1/c$ monoclinic spacegroup, finding a statistically significant improvement in fit on adopting this model.

Each of the studies outlined previously have focussed on discrete compositions and have not, as yet, investigated the oxidation of $Sr_2MnO_{3.5+x}$ using *in-situ* characterisation techniques. One study has inferred oxidation behaviour from analysis of thermal expansion behaviour[20], but no structural data was reported. It is the intention of this study to detail the oxidation behaviour of $Sr_2MnO_{3.5+x}$ using *in-situ* neutron diffraction techniques and to determine the temperature at which oxidation in air occurs.

2. Experimental

Samples of composition $Sr_2MnO_{3\pm x}$ were prepared using standard solid state synthesis techniques as previously suggested[6, 19]. Stoichiometric quantities of $SrCO_3$, (Alfa Aesar, 99.999%) and MnO_2 (Alfa Aesar, 99.999%) were intimately ground in an agate mortar and pestle under acetone and allowed to air dry. Powder samples were pressed into 10mm diameter disks and were then heated to 1300 ^oC under flowing Argon for a period of 12 hrs in alumina crucibles before cooling to ambient temperature (25 ^oC). Samples were further reground and examined by powder X-ray diffraction (Phillips PW 1700 series diffractometer, Cu K_α radiation (λ = 1.5409Å), Si single crystal secondary monochromator) to determine if single phase materials had formed and the heat treatment process repeated until a single phase was present.

Preliminary *in-situ* X-ray powder diffraction data were collected on a Siemens D5000 diffractometer using Cu K_α radiation with an Anton Paar high temperature stage. High resolution X-ray diffraction data were obtained for the as-prepared $Sr_2MnO_{3.5+x}$ samples at room temperature on station 2.3 at the Daresbury Laboratory with a step size of 0.01 at a wavelength of 1.301Å. Powder neutron diffraction data were collected on the D2B beamline at the Institut Laue Laugevin (ILL), Grenoble, France, at a wavelength of 1.594 Å. Samples (~3g) were contained in quartz ampoules open to a static air environment to ensure oxidation would occur. Full diffraction patterns (5-160^o 2θ) over the temperature range 200 – 375 ^oC on both heating and cooling were obtained. Data from the D2B beamline were recorded over a time period of 3 hours. Resulting diffraction patterns were refined with the Topas suite of software[24] using the JEdit routines developed at the University of Durham[25]. A significant background was observed, originating from the quartz ampoule used to contain the sample in the neutron beamline. The background function used in each refinement was expanded to account for this.

3. Results and Discussion

From the synchrotron XRD data presented in Figure 1, it was clear that single phase material had successfully been produced through the solid state synthesis route which on initial inspection appeared to match the reported tetragonal structure of Sr_2MnO_4[23]. Further investigation of this data using Rietveld refinement indicated that, rather than the tetragonal cell, a good fit to a monoclinic cell with a = 6.8541(2), b = 10.8113(3), c = 10.8142(3) Å and β = 113.25(4)^o was achieved, in agreement with the parameters reported by Gillie *et al*[19] determined from a neutron diffraction study. Preliminary examination of the *in-situ* X-ray

powder diffraction data indicated that significant changes in the lattice occurred on heating the as-prepared $Sr_2MnO_{3.5+x}$ powders in air, Figure 2. A shift of the Bragg peaks to higher angle is clear in the temperature window 28-348 ^oC but it is also evident that a considerable broadening of the peaks at high angle (> 65^o 2θ) occurs, accompanied by the development of peak asymmetry. Due to this significant broadening it was not possible to refine the X-ray data to a structural model and therefore ascertain whether a structural change was occurring or simply that the kinetics of the oxidation process were such that over the period of the diffraction measurement a number of variable stoichiometry phases were coexisting giving rise to variable lattice parameters which were averaged over the measurement time resulting in several overlapping peaks. Evidently the incorporation of oxygen into the lattice is likely to be the source of these changes, but oxygen effects are difficult to determine from X-ray powder diffraction data.

To attempt to resolve these issues neutron diffraction data were obtained as a function of temperature over a limited temperature range on the D2B high resolution beamline at the ILL. Initial inspection of the diffraction patterns obtained in a static air atmosphere at temperatures from 200 – 375 ^oC indicated no significant differences in the data, but on closer inspection there were clear differences in peak positions, intensities and shapes at higher angles, Figure 3. Previous data reported by Gillie et al[19] proposed a monoclinic unit cell for $Sr_2MnO_{3.5}$, rather than the more commonly suggested tetragonal *I4/mmm* model[20]. In the current work we have used both models at all temperatures and find that, in agreement with the room temperature structure proposed by Gillie, the data obtained at 207 ^oC is indeed monoclinic with the $P2_1/c$ space group identified for the room temperature data and cell parameters of a = 6.8657(2), b = 10.8319(5), c = 10.8384(5) Å and β = 113.283(4). A typical fitted powder pattern is displayed in Figure 4 with the refined data displayed in Table 1. In the refinement, as discussed previously[19], certain isotropic temperature factors have been fixed to a slight positive value as these positions had a tendency to refine to meaningless values. This may be partially attributed to a distorted environment around the Mn1 position due to the incomplete occupancy of the O4 position.

On heating it was observed that the material underwent a significant oxidation process, leading to a clear shift in peak position to higher angles. These observations indicated that the oxidised phase was structurally similar to the reduced material and that there were no significant structural changes occurring on heating. Therefore the cell expansion would be due directly to the incorporation of oxygen species. Through repeated refinements to both proposed tetragonal and monoclinic unit cells it has been determined that the unit cell under goes a structural modification from the monoclinic $P2_1/c$ to the tetragonal *I4/mmm* cell on

heating, with associated oxidation of the Mn species from Mn^{3+} to Mn^{4+}. Currently it is unclear at precisely which temperature the transition takes place, but it appears to evolve over a wide temperature range and thus is clearly a complex process involving the gradual filling of the vacant oxygen lattice sites. However it is clear that this oxidation process does not occur homogeneously throughout the sample and hence a phase mixture results. It is evident that the onset of the oxidation is approximately 275^{o}C and that the phase transformation associated with the oxidation is complete on cooling from 375^{o}C. From the data obtained it is possible to fit to the monoclinic cell at temperatures below 325^{o}C, however at this temperature the powder pattern appears to have an intermediate character between the low temperature reduced monoclinic and higher temperature oxidised tetragonal structures. This observation is clear in Figure 5 where the peaks at between 130 and 135^{o} 2θ are "smeared", with the broadening due either to a new phase or a combination of several structurally similar, but with potentially different oxygen stoichiometry, phases. It is feasible that this may be due to a mixture of tetragonal and monoclinic phases but refinements of this mixture were unsuccessful. This indicates that the phase mixture is more complex than initial inspection indicates. Unfortunately the data collection time required for these samples with the D2B diffractometer was not sufficient to fully resolve these features.

At temperatures above 325^{o}C the data refines well to the tetragonal structure with no improvement in the fitting parameters on refining the data to the monoclinic cell. On cooling from 375^{o}C to room temperature after oxidation the material remains tetragonal in structure adopting the *I4/mmm* spacegroup, Figure 6 and Table 2, and therefore the oxidation process is not, under static air, reversible.

From the refinements we calculate that the oxygen stoichiometry of the as-prepared (reduced) materials at 207^{o}C is d = 3.61 (where d = total oxygen content) which increases steadily with heating until a final stoichiometry of d = 3.96 is achieved at 375^{o}C. Further heating beyond 375^{o}C may induce an increase in oxygen content but it is clear from examination of Figure 8 that there is no further structural change associated with heating beyond 375^{o}C. On cooling there is no further significant oxidation and no evidence of reversibility. This oxidation process is clearly illustrated in Figure 7. Oxidation of the Sr_2MnO_{3+x} phases upon heating in air is not unexpected and the data reported here confirm the oxidation process. However the nature of the oxidation is of interest and it is clearly not a simple process. From Figure 9 an obvious broadening of the peak at ~ 69^{o} 2θ is observed at between 325 and 375^{o}C on heating, and significant asymmetry is present, indicating that more than one phase could be present, although refining these data has proved virtually impossible.

The data for the reduced phase of Sr_2MnO_{3+x} clearly demonstrates that a monoclinic structure is maintained on heating in air until at least 275°C at which point oxidation is initiated, with the calculated lattice parameters given in Table 3. On heating above the oxidation onset temperature and on further cooling, the tetragonal structure and increased oxygen content is maintained. These structural transitions are governed by the change in the valence of the Mn^{3+} species to the Mn^{4+} species and the associated filling of the partially occupied O4 position on oxidation.

Changes in the coordination environment are clear from a consideration of the bond distances for the two structures. Tables 4 and 5 present these data for three samples: 325°C on heating (tetragonal refinement), 275°C on cooling (tetragonal) and 207°C on heating (monoclinic) showing that the calculated bond lengths for the monoclinic sample at 207°C are in good agreement with those previously reported[19] for room temperature measurements. It is of interest to note that the coordination of the monoclinic sample, Table 4, is effectively Mn-O_5 with the oxidation filling the partially occupied 6th oxygen position. It is also clear that the Mn-O environments are only fractionally non-octahedral, with most bonds ~1.95Å. The bonds that vary significantly from this are Mn1-O4 (2.10Å), Mn2-O4 (1.80Å) which are both associated with the partially occupied oxygen site, and the Mn2-O2 bond (1.74 Å). On transition to the tetragonal polymorph the coordination environment becomes a distorted octahedron, with two long Mn-O apical bonds at ~1.95Å and with four equatorial bonds of ~1.90Å. The distortion of the octahedral coordination is commonly observed in Ruddlesden-Popper type phases with variable valence B site cations, often attributed to Jahn-Teller distortion. In systems with Mn^{3+} cations Jahn-Teller distortion of the Mn-O_6 octahedra is highly likely. From Table 3 it is clear that on cooling there is a contraction of the Mn-O bonds in both apical and equatorial positions of the octahedra, as would be expected through thermal expansion/contraction, with the equatorial bond distances corresponding to the *a* lattice parameter. Considering the ratio of the Mn-O_{ap}/Mn-O_{eq} it is found that although the overall bond lengths decrease on cooling, the ratio also decreases, from 1.035 to 1.025, indicating that the MnO_6 octahedron is becoming slightly less distorted. This coincides with an increase in the average Mn valence from 3.40+ to 3.92+, calculated from the oxygen non-stoichiometry, and hence a lowering of the Jahn-Teller distortion.

The rapid oxidation of the $Sr_2MnO_{3.5+x}$ phase indicates that the incorporation of oxygen is facile with the charge compensation maintained through the filling of vacant oxygen positions:

$$2Mn_{Mn}^{x} + V_O^{\bullet\bullet} + \tfrac{1}{2}O_{2(g)} \rightarrow 2Mn_{Mn}^{\bullet} + O_O^{x}$$

and hence there is no significant change in the conduction properties of this material. However there have been reports of substituted phases such as $Sr_{2-x}La_xMnO_4$ being used for fuel cell electrodes[26] and it is likely that the active surfaces are of significance in these applications.

Conclusions

$Sr_2MnO_{3.5+x}$ phases have been prepared in their reduced (predominantly Mn^{3+}) polymorph and the evolution of the structure on oxidation investigated using *in-situ* diffraction techniques. Oxidation is clearly a rapid process beginning at a relatively low temperature of 275^{o}C, and complete by 375^{o}C. No major structural changes were observed, but a subtle phase evolution was identified through Rietveld refinement of neutron powder diffraction data. A monoclinic cell was fitted to the data obtained for the as-prepared material, with a transition to a tetragonal cell found at temperatures in excess of 275^{o}C coincident with significant oxidation (Mn^{3+} to Mn^{4+}). On achieving full oxidation the tetragonal phase was stabilised and no reversibility was observed. It was evident that the oxidation step was more rapid than that time resolution of the diffractometer and hence the surface incorporation of oxygen is a rapid process.

Acknowledgements

We are indebted to the Institut Laue Langevin (ILL), Grenoble, France for the grant of experiment time on the D2B beamline. We also thank Dr Emma Suard, Station Scientist on D2B, for her invaluable assistance in setting up the experiment. For access to the XRD beamline at Daresbury Laboratory, UK, we thank the EPSRC and Dr Chiu Tang, for assistance with set-up and data collection. Further thanks are due to Professor Rose-Noelle Vannier at ENSC Lille for access to high temperature *in-situ* XRD. Finally we thank the British Council and National Research Council Canada, NERC and EPSRC for funding studentships (CNM, RS and PAS).

References

1. Mauvy, F., Lalanne, C., Bassat, J. M., Grenier, J. C., Zhao, H., Dordor, P. and Stevens, P., *J. Eur. Ceram. Soc.* **2005,** 25, 2669-2672.
2. Lalanne, C., Prosperi, G., Bassat, J. M., Mauvy, F., Fourcade, S., Stevens, P., Zahid, M., Diethelm, S., Van Herle, J. and Grenier, J. C., *J. Power Sources* **2008,** 185, 1218-1224.
3. Weng, X. L., Boldrin, P., Abrahams, I., Skinner, S. J. and Darr, J. A., *Chem. Mater.* **2007,** 19, 4382-4384.
4. Tarancon, A., Skinner, S. J., Chater, R. J., Hernandez-Ramirez, F. and Kilner, J. A., *J. Mater. Chem.* **2007,** 17, 3175-3181.
5. Skinner, S. J., *Solid State Sci.* **2003,** 5, 419-426.
6. Munnings, C. N., Skinner, S. J., Amow, G., Whitfield, P. S. and Davidson, I. J., *Solid State Ionics* **2006,** 177, 1849-1853.
7. Battle, P. D. and Rosseinsky, M. J., *Current Opinion in Solid State & Materials Science* **1999,** 4, (2), 163-170.
8. Battle, P. D., Branford, W. R., Mihut, A., Rosseinsky, M. J., Singleton, J., Sloan, J., Spring, L. E. and Vente, J. F., *Chem. Mater.* **1999,** 11, 674-683.
9. Battle, P. D., Green, M. A., Laskey, N. S., Millburn, J. E., Radaelli, P. G., Rosseinsky, M. J., Sullivan, S. P. and Vente, J. F.,. *Phy. Rev. B* **1996,** 54, 15967-15977.
10. Greenblatt, M., *Current Opinion in Solid State & Materials Science* **1997,** 2, (2), 174-183.
11. Puche, R. S., Norton, M. and Glaunsinger, W. S., *Mater. Res. Bull.* **1982,** 17, 1429-1435.
12. Lehuede, P. and Daire, M., *Comptes Rendus De L Academie Des Sciences Serie C* **1973,** 276, 1011-1013.
13. Greene, R. L., Maletta, H., Plaskett, T. S., Bednorz, J. G. and Muller, K. A., *Solid State Commun.,* **1987,** 63, 379-384.
14. Poirot, N. J., Odier, P. and Simon, P., *J. Alloys Compds.,* **1997,** 262, 147-151.
15. McCormack, M., Jin, S., Tiefel, T. H., Fleming, R. M., Phillips, J. M. and Ramesh, R., *Appl. Phys. Lett.* **1994,** 64, 3045-3047.
16. Jin, S., McCormack, M., Tiefel, T. H. and Ramesh, R., *J. Appl. Phys.* **1994,** 76, 6929-6933.
17. Dulli, H., Dowben, P. A., Liou, S. H. and Plummer, E. W., *Phys. Rev. B* **2000,** 62, 14629-14632.
18. Kato, C., Iikubo, S., Soda, M., Sato, M., Kakurai, K. and Yoshii, S., *J. Phys. Soc. Jpn* **2005,** 74, 1026-1029.
19. Gillie, L. J., Wright, A. J., Hadermann, J., Van Tendeloo, G. and Greaves, C., *J. Solid State Chem.* **2002,** 167, 145-151.
20. Kriegel, R. and Preuss, N., *Thermochimica Acta* **1996,** 285, (1), 91-98.
21. Kriegel, R., Borrmann, H., Simon, A. and Feltz, A., *Zeitschrift Fur Naturforschung Section B-Journal of Chemical Sciences* **1993,** 48, 15-18.
22. Li, R. K. and Greaves, C., *J Solid State Chem.* **2000,** 153, 34-40.
23. Bouloux, J. C., Soubeyroux, J. L., Leflem, G. and Hagenguller, P., *J Solid State Chem.* **1981,** 38, 34-39.
24. Coelho, A. A., TOPAS v4.1: General Profile and Structure Analysis Software for Powder Diffraction Data. In 2008.
25 Evans, J.S.O, Dept. of Chemistry, University of Durham, Durham, UK, http://www.dur.ac.uk/john.evans/topas_academic/topas_main.htm
26 Sun LP, Huo LH, Zhao H, Li Q, Pijolat C., J. Power Sources, **2008**, 179, 96-100

List of Figures

Table 1 – Atomic positions of monoclinic $Sr_2MnO_{3.5+d}$ recorded at 207°C. Note B_{eq} fixed for Mn1, O2 and O4. Fractional occupancies were initially refined and found to be unity. Subsequent refinements used fixed values to limit the number of free parameters.

Atom	x	y	z	Occ	B_{eq}
Sr1	0.291(3)	-0.009(2)	0.071(3)	1	0.64
Sr2	0.298(3)	-0.002(2)	0.579(3)	1	0.66
Sr3	0.296(3)	0.254(3)	0.333(3)	1	0.89
Sr4	0.292(3)	0.755(2)	0.315(2)	1	0.31
Mn1	0.003(5)	-0.005(3)	0.247(4)	1	0.01
Mn2	-0.003(6)	0.243(3)	-0.012(3)	1	0.08
O1	-0.017(6)	0.128(4)	0.109(4)	1	2.34
O2	0.009(5)	0.105(2)	0.391(2)	1	0.01
O3	-0.005(6)	0.131(3)	0.868(3)	1	1.45
O4	0.000(19)	0.159(9)	0.637(8)	0.217(28)	0.01
O5	0.314(3)	-0.005(2)	0.336(5)	1	0.27
O6	0.315(5)	0.008(2)	0.827(4)	1	1.21
O7	0.301(4)	0.259(4)	0.086(3)	1	0.95
O8	0.311(5)	0.736(3)	0.067(3)	1	0.63

Table 2 – Refined atomic positions for the tetragonal modification of $Sr_2MnO_{3.5+x}$ on (a) heating to 325°C and (b) cooling to 275 °C

$Sr_2MnO_{3.5+x}$ at 325°C on heating

Atom	x	y	z	occ.	B_{eq}
Sr	0	0	0.3554(3)	1	0.84(8)
Mn	0	0	0	1	0.40(13)
O1	0	0.5	0	0.85(1)	1.22(11)
O2	0	0	0.1574(4)	1	0.85(9)

$Sr_2MnO_{3.5+x}$ at 275°C on cooling

Atom	x	y	z	occ.	B_{eq}
Sr	0	0	0.3554(2)	1	0.84(3)
Mn	0	0	0	1	0.32(7)
O1	0	0.5	0	0.98(1)	0.77(4)
O2	0	0	0.1555(2)	1	0.80(4)

Table 3 – Refined lattice parameters for all samples recorded as a function of temperature. Note e.s.d. values are higher for those samples around the transition region. Angles for the tetragonal phases are all 90° and hence not included in the table.

Temperature / °C	a / Å	b / Å	c / Å	β
207	6.8656(3)	10.8320(4)	10.83834(4)	113.281(4)
275	6.8667(8)	10.8417(14)	10.8420(12)	113.229(4)
325	3.8164(4)	3.8164(4)	12.5595(16)	
375	3.8126(2)	3.8126(2)	12.5627(8)	
325	3.80846(5)	3.80846(5)	12.5519(2)	
275	3.80562(4)	3.80562(4)	12.5438(2)	

Table 4 – Bond lengths for tetragonal composition at 325°C and 275°C (cooling) respectively

Temp./°C	Bond	Distance /Å	No.
325	Sr-O	2.487(6)	1
		2.634(3)	4
		2.7034(5)	4
	Mn-O	1.90818	4
		1.976(5)	2
275 (cooling)	Sr-O	2.507(3)	1
		2.629(1)	4
		2.6944(2)	4
	Mn-O	1.90279	4
		1.950(3)	2

Table 5 – Bond distances for the monoclinic structure determined from Rietveld refinement of data recorded at 207°C.

Bond	Distance / Å
Mn1-O1	2.05(5)
Mn1-O2	1.96(5)
Mn1-O3	1.85(5)
Mn1-O5	1.97(4)
Mn1-O6	2.01(4)
Mn1-O4	2.10(9)
Mn2-O1	1.74(5)
Mn2-O2	2.05(4)
Mn2-O3	1.98(5)
Mn2-O7	1.92(6)
Mn2-O8	1.96(6)
Mn2-O4	1.80(10)

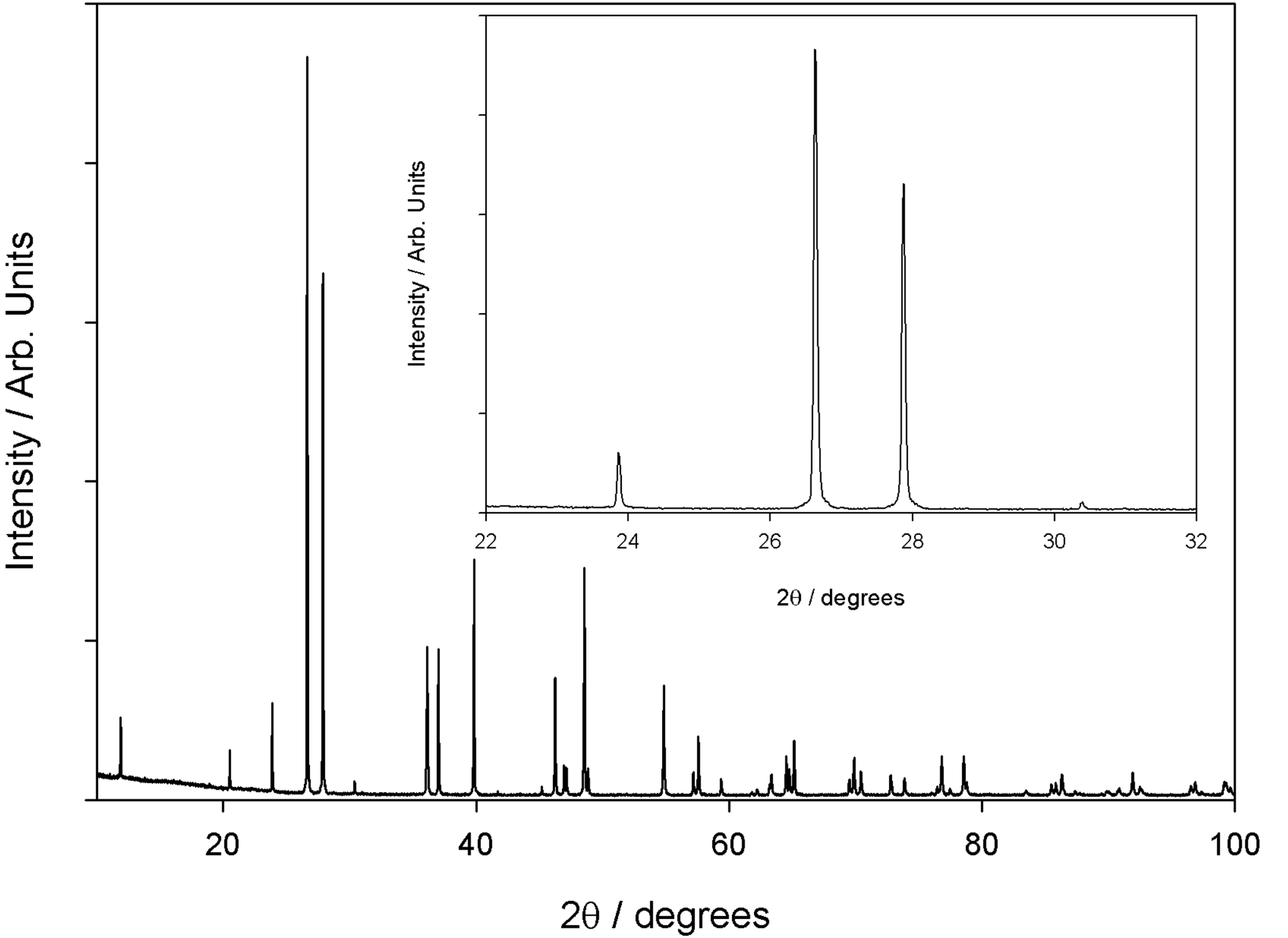
Intensity / Arb. Units
20
40
60
80
100
2θ / degrees
Intensity / Arb. Units
22
24
26
28
30
32
2θ / degrees

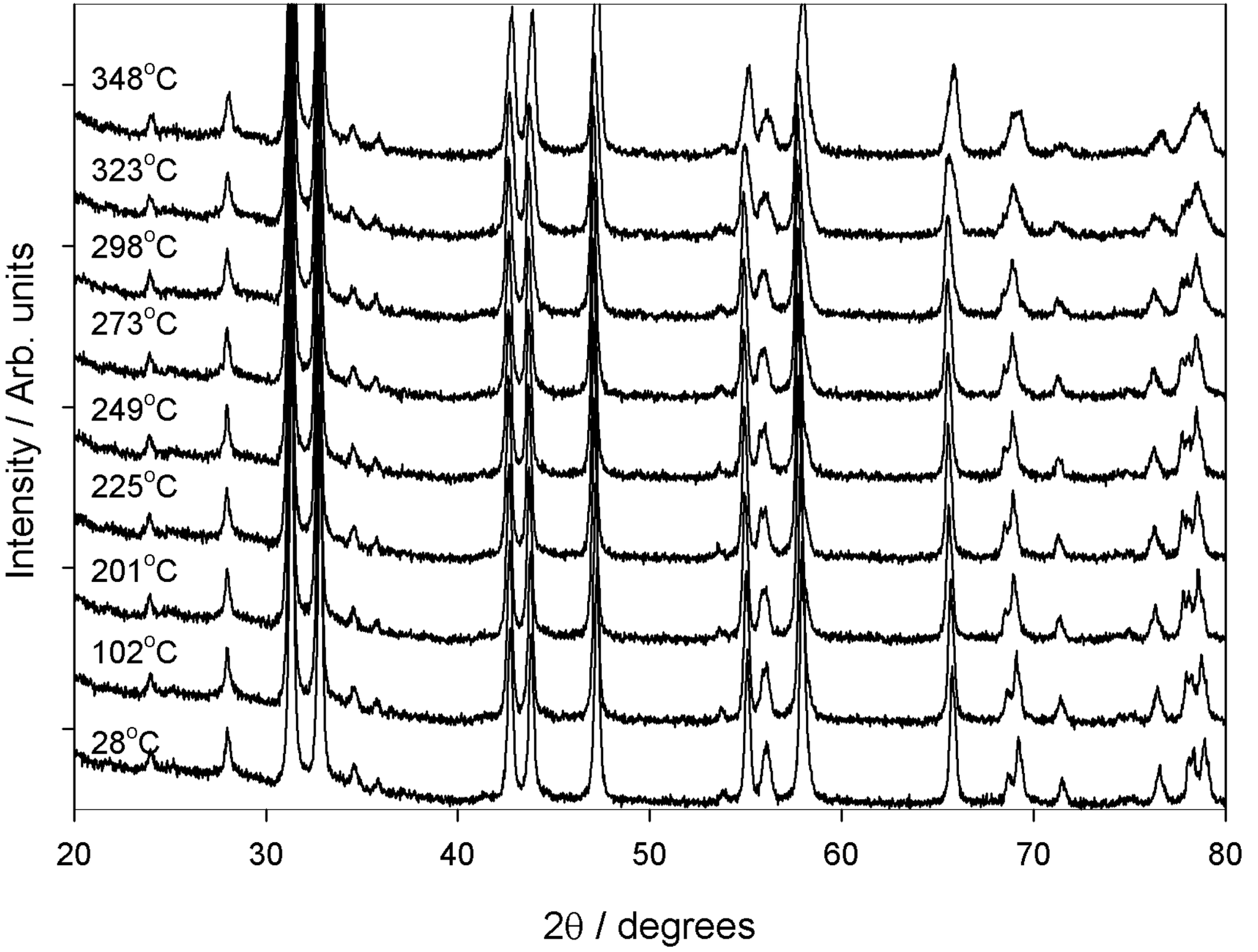
348°C
323°C
298°C
273°C
249°C
225°C
201°C
102°C
28°C
Intensity / Arb. units
20
30
40
50
60
70
80
2θ / degrees

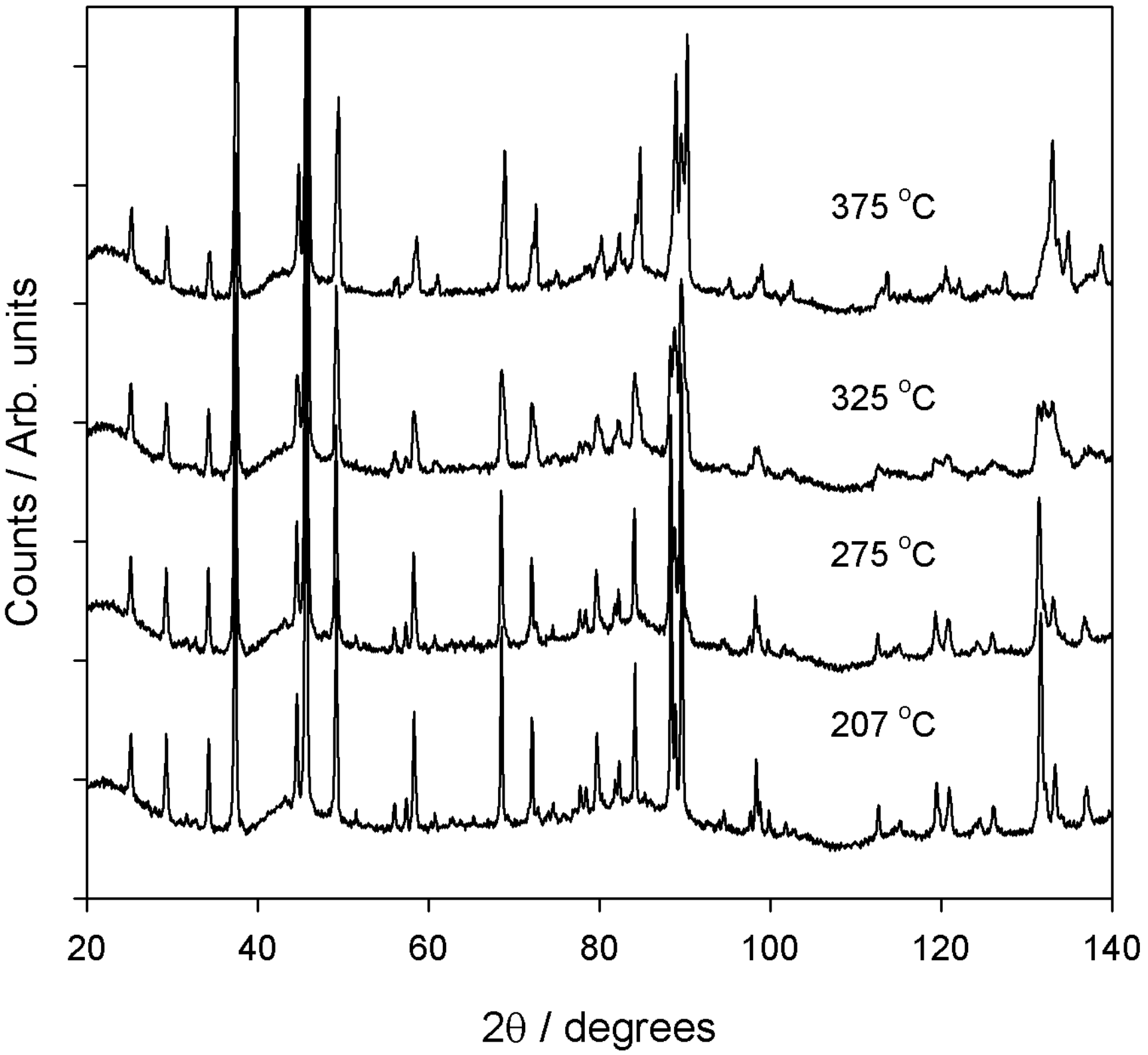
375 °C
325 °C
275 °C
207 °C
Counts / Arb. units
20
40
60
80
100
120
140
2θ / degrees

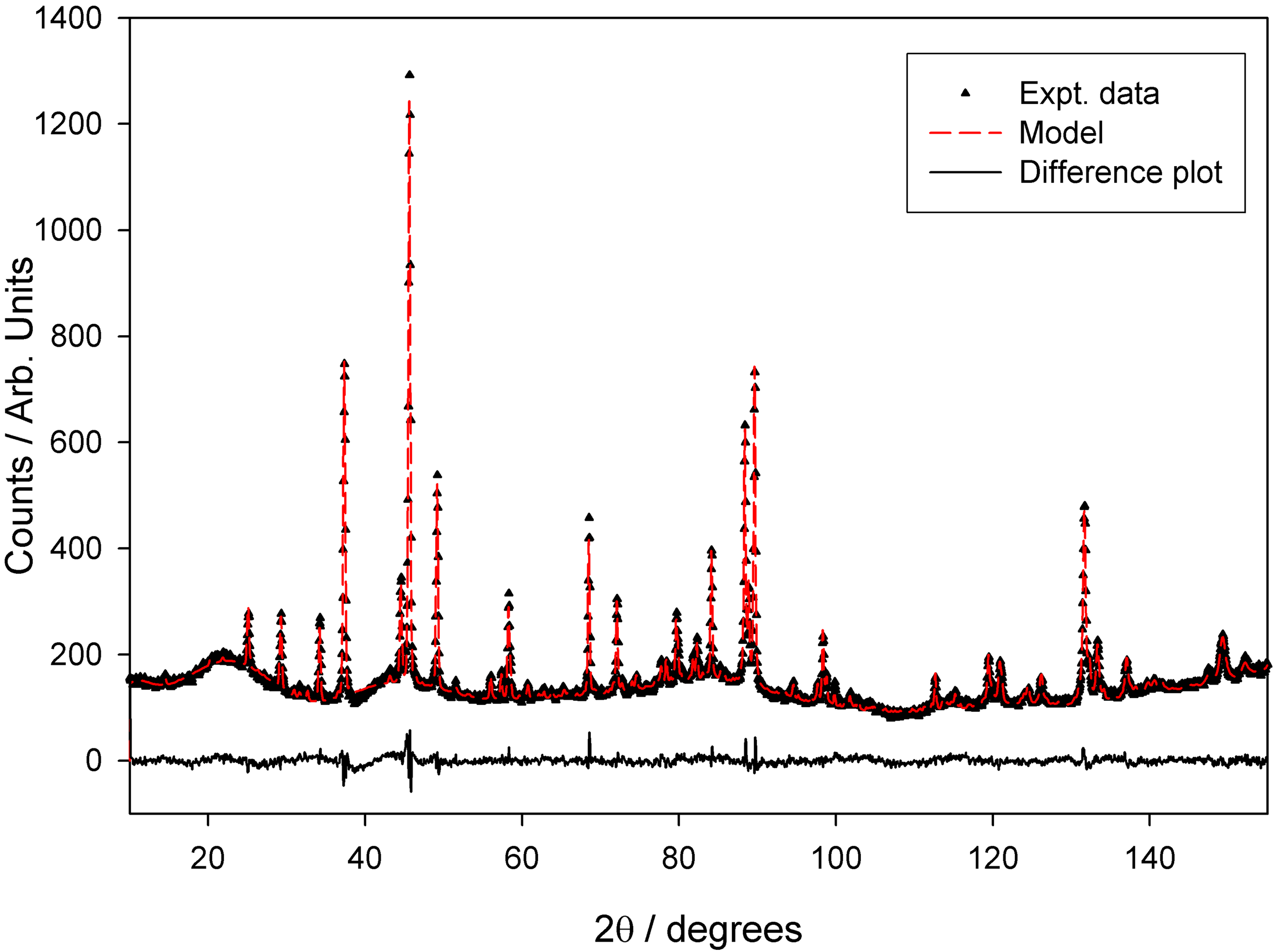
Expt. data
Model
Difference plot
Counts / Arb. Units
0
200
400
600
800
1000
1200
1400
20
40
60
80
100
120
140
2θ / degrees

(3 1 10)
(3 3 4)
(4 2 0)
275 °C
325 °C
375 °C
325 °C
275 °C
207 °C
Counts / Arb. units
126
128
130
132
134
136
138
140
142
2θ / degrees

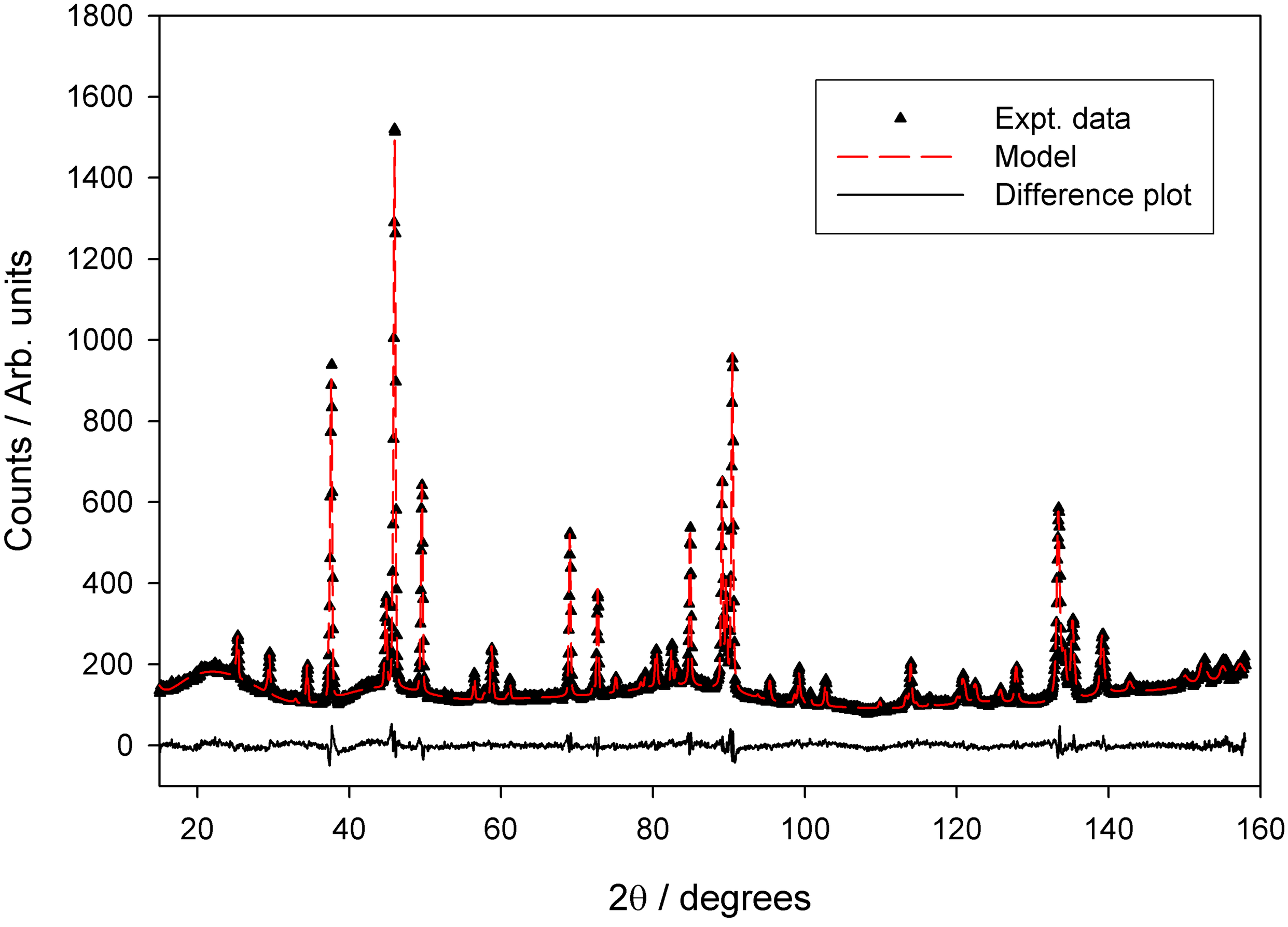
Expt. data
Model
Difference plot
Counts / Arb. units
1800
1600
1400
1200
1000
800
600
400
200
0
20
40
60
80
100
120
140
160
2θ / degrees

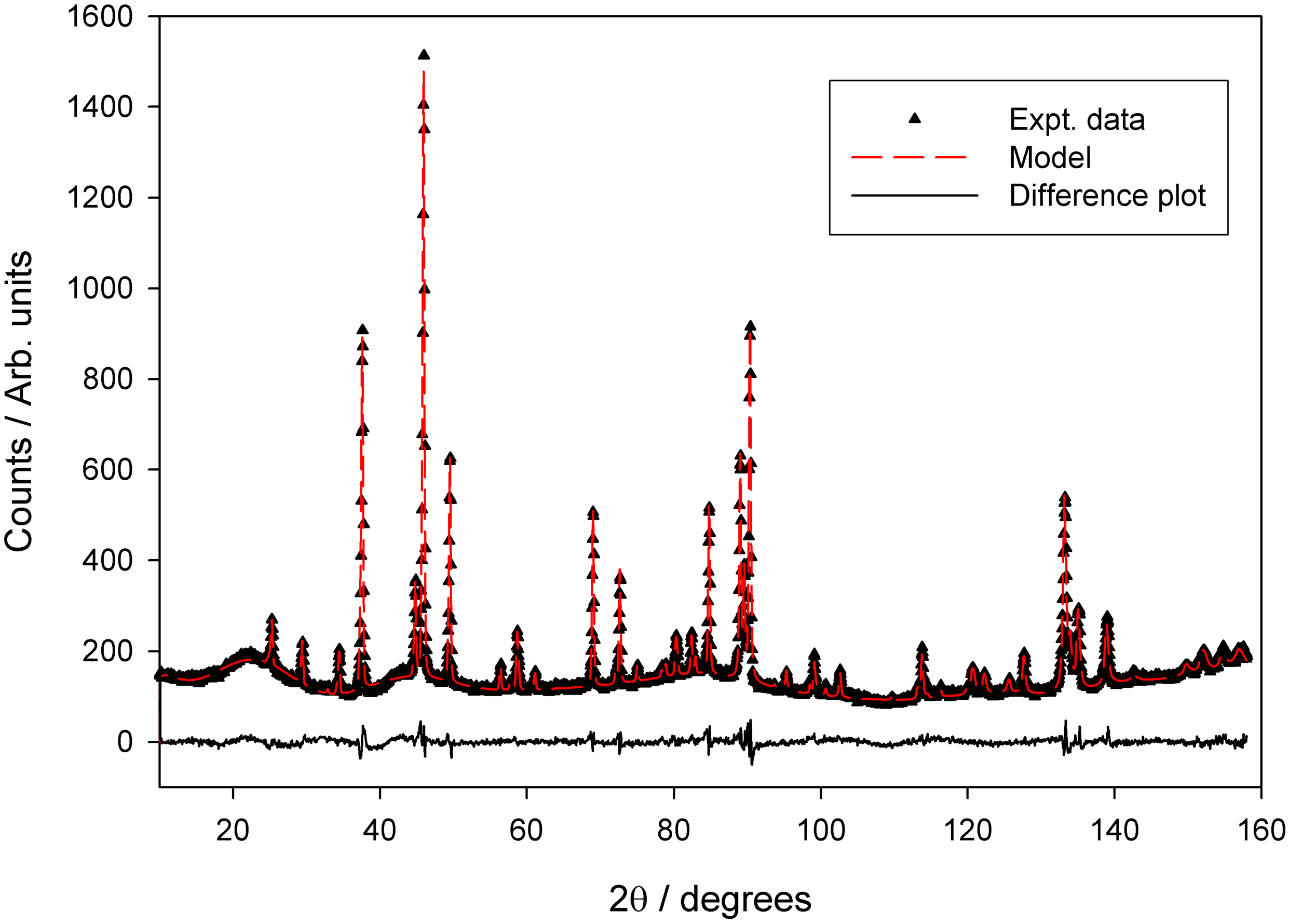
Counts / Arb. units
1600
1400
1200
1000
800
600
400
200
0
20
40
60
80
100
120
140
160
2θ / degrees
Expt. data
Model
Difference plot

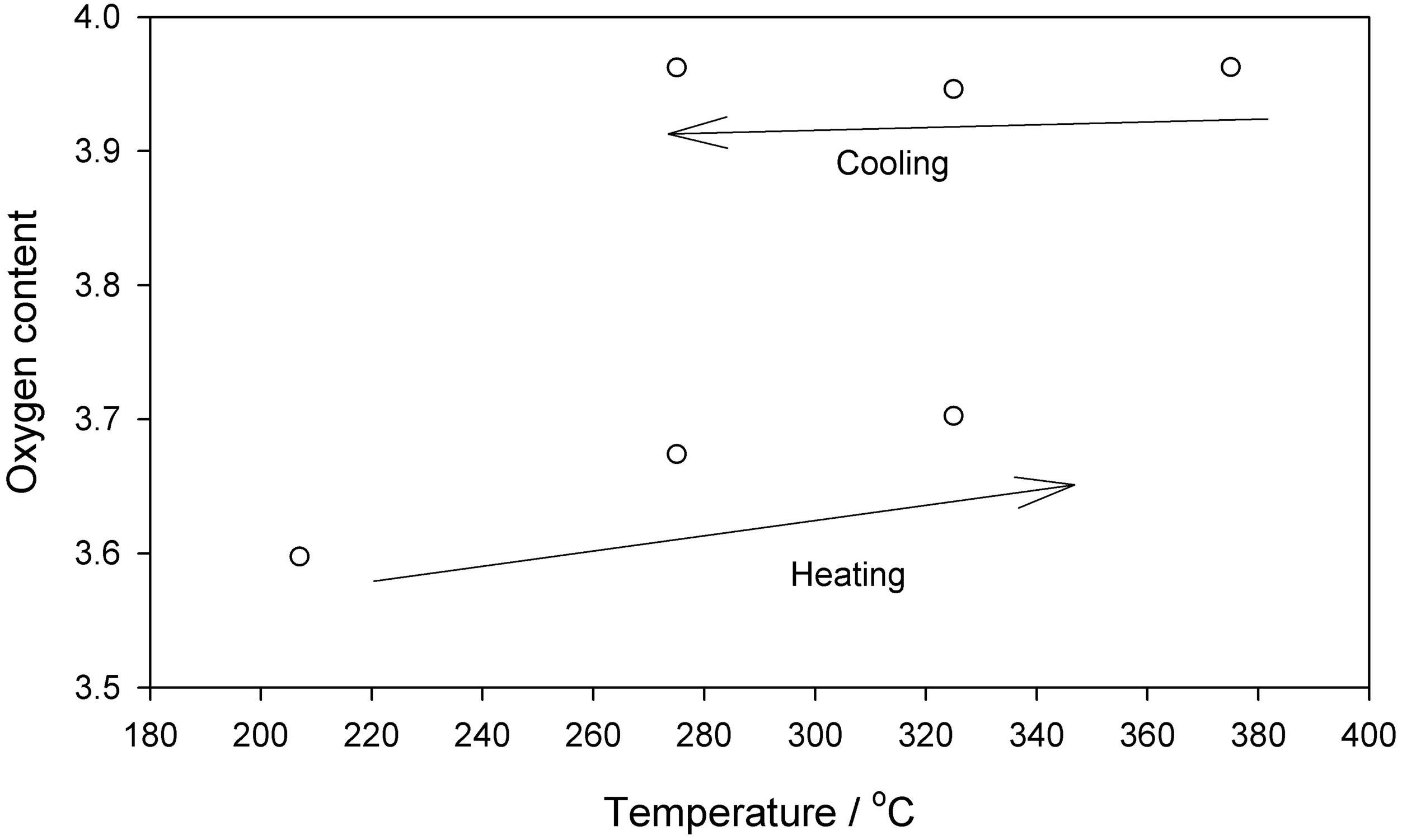
4.0
3.9
3.8
3.7
3.6
3.5
Oxygen content
Cooling
Heating
180
200
220
240
260
280
300
320
340
360
380
400
Temperature / °C

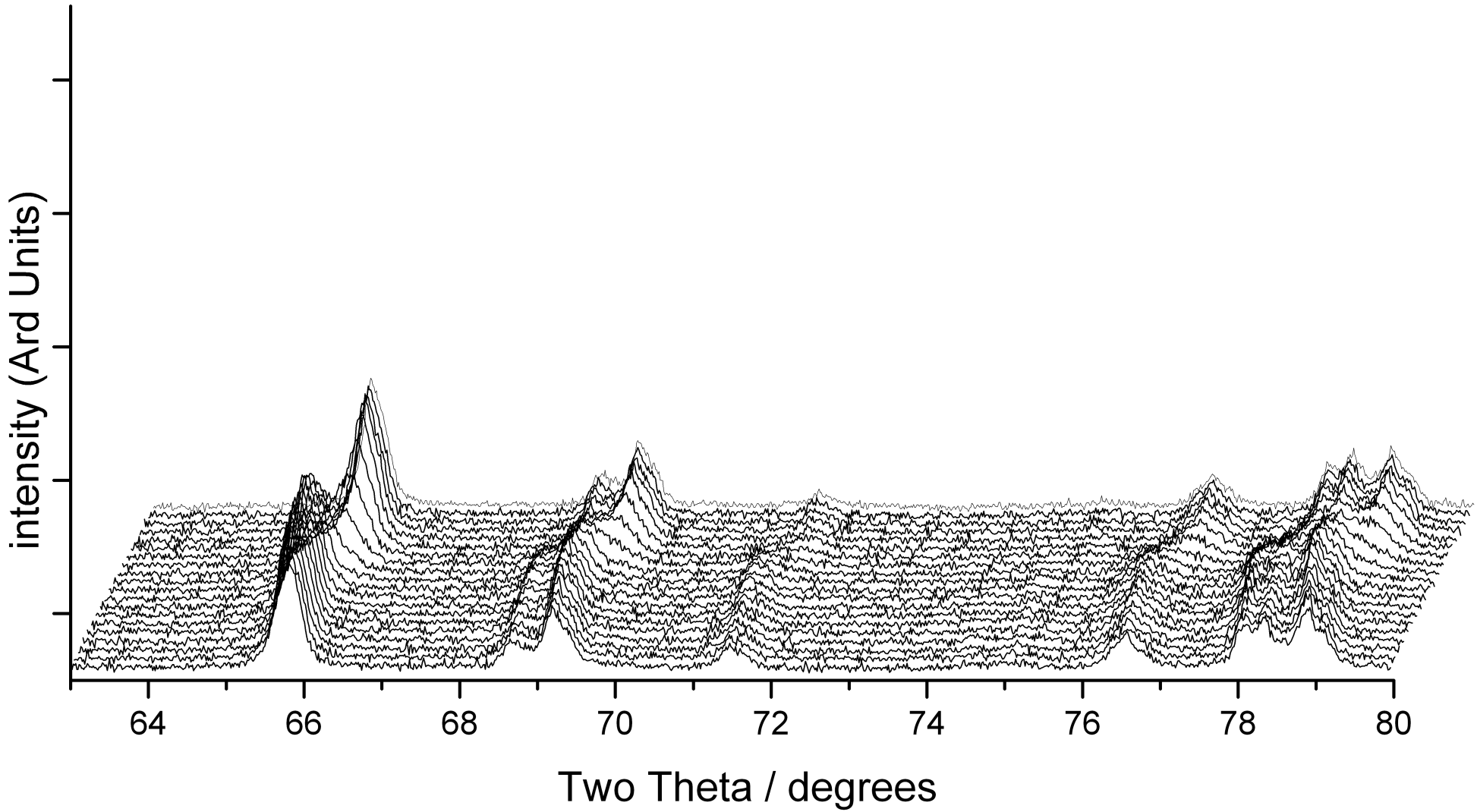
intensity (Ard Units)
64
66
68
70
72
74
76
78
80
Two Theta / degrees

(2 1 5)

275 °C

325 °C

375 °C

325 °C

275 °C

207 °C

Counts / Arb. units

67.0

67.5

68.0

68.5

69.0

69.5

70.0

2θ / degrees